

Numerical Study of Unsteady Flow Separation on Small Scale Wings Using Vortex Identification Methods

Viet Anh Duong¹, Viet Dung Duong^{2*}

¹University of Science and Technology of Hanoi, Vietnam Academy of Science and Technology, Ha Noi, Vietnam

²School of Aerospace Engineering, VNU University of Engineering and Technology, Ha Noi, Viet Nam

*Corresponding author email: duongdv@vnu.edu.vn

Abstract

The goal of this work is to develop vortex identification methods for better understanding the unsteady separation using particle-based direct numerical simulation for the unsteady incompressible flow past small wings. It is shown that in flows with Reynolds number 1000, the first vortex identification method, vorticity contour, is used to capture the vortical region behind the surface in which the package of unsteady vortex bubbles is observed in different angles of attack. The second vortex identification method, Q -criterion, has shown the advantages in order to capture the vortical region and track the near-wall separation by recording the vortex strengths of leading edge vortex and trailing edge vortex at high angle of attacks. The time history of the strengths has shown a good agreement to the time history of drag coefficient. The third vortex identification method, Lagrangian coherent structure, has shown its strength to record the most stretching, attracting, and shearing material surfaces that form the skeletons of Lagrangian particle dynamics in the far-field wake region. Accordingly, the tracking of particles in high shear surfaces, which is very important to determine the roadmap of unsteadiness, is well captured.

Keywords: Unsteady laminar Separation, vortex method, vortex identification, Lagrangian coherent structure.

1. Introduction

To better understand bird and insect flight as well as to model the advanced aerodynamic effects for micro-aerial vehicles (MAVs), see [1-3], the need to study low Reynolds number ($\leq 10^4$) aerodynamics associated with flow over low aspect ratio thin wings, such as airfoil and flat plate, is driven. For this range of Reynolds numbers, the flow initially forms a laminar boundary layer around the surface. The laminar boundary layer gradually separates from the surface. The separated flow ultimately forms a separation bubble (SB), which can be periodically shed downstream. The formation of the SB is due to the effect of an adverse pressure gradient. Such bubbles are typically observed in the region close to the leading edges of thin wings on micro-aero-vehicle wings, see [4], or on insect's wings [5].

The unsteady separation bubble produces a significant effect to either enhance or decrease lift depending on the effective shape of the airfoil and specific maneuver. The attachment and development of the SB to the wings causes the temporarily enhanced lift and decreased pitching moment while the reattachment influences the aerodynamic performance, generally in a negative manner. The understanding of the physics of the SB and possible

ways to control it thus is the preliminary need for efficient design of these aerodynamic devices.

Experimental investigations of this separated flow are very important due to accuracy. However, this usually takes time and also it is very costly. With the explosive growth in the computer industry there has been a tremendous increase in the computing power and speed. Therefore, now the shift is towards computer modeling of the separation bubble by using the principles of Computational Structural Dynamics and the Advanced Computational Fluid Dynamics (CFD). Obviously, the computational attempts reduce cost and time.

The aim of this research is to better understand the unsteady laminar separation, which is found in the design of high-performance micro-aerial vehicles and observations of bird and insect flight by performing a cheap and reliable study. For this purpose, the direct numerical simulation solver, see [6], is used to investigate two-dimensional viscous incompressible flow past the airfoil (NACA 0012) at different ranges of angle of attack (AoA). The advanced CFD solver is named the purely Lagrangian vortex method. The no-slip boundary condition is explicitly enforced by releasing wall vortex blobs at each time step based on representation of Nascent vortex elements. Viscous effect is modeled by core spreading method (CSM) with Splitting and Merging spatial adaptation scheme.

Velocity field is calculated by using Biot-Savart formulation. For acceleration of the velocity computation, the Fast Multipole Method (FMM) is also employed.

Moreover, due to the significant roles of vortical structures in turbulence, research for vortex identification has been interesting. It has come up with a number of methods which are designed to identify vortices given the output of simulations or velocity measurements in experiments, see [7] and [8]. Recently, identification of vortices plays an important role for understanding complex flow phenomena, see [9]. In addition, the vortical structures are also found in studies of unsteady laminar separation, see [10]. Hence, the aim of this paper is to develop several vortex identification methods for the direct numerical simulation data to extract more information of the unsteady separation process which is found in engineering design of micro air vehicles.

To the best of the authors' knowledge, the previous studies have not performed the unsteady flow separation, where the complex vortex structures are highly concerned. In order to detect the physics of these structures, the identification methods are required. Therefore, this study proposes three vortex identification methods, including vorticity, Eulerian, and Lagrangian methods. This paper is organized as follows. The first section is the introduction and background. The second section is the performance of three vortex identification methods to visualize the unsteady vortical region of flow over an airfoil with different angle of attack. The setup of a numerical experiment and the convergence study are performed in this section. The last section is the records of aerodynamic forces in order to reconfirm those observations in the second section.

2. Fast Lagrangian Vortex Method

The work that follows relies on fully resolved direct numerical simulations performed using a fast lagrangian vortex method developed at Institut Teknologi Bandung [6]. With this code, it is possible to construct incompressible flow experiments at low Reynolds numbers (< 1000) and obtain velocity snapshots of the flow field. The method efficiently solves the incompressible Navier-Stokes equations using a fractional step method on a set of particles scattered around the body. Typically, a convergence study is performed by setting the finest and coarsest resolutions as $\sqrt{6\nu\Delta t}$ and $\sqrt{15\nu\Delta t}$ core size of particle, respectively. The kinematic viscosity ν is calculated based on Reynolds number as $\nu = UD/Re$, where U and D are characteristic velocity and length. The convergence study is also performed at $Re = 1000$ for a stationary airfoil NACA 0012 with an AoA $\alpha = 50^\circ$, length $D = 1$ (chord length of NACA 0012) and incremental time $\Delta t = 0.01$.

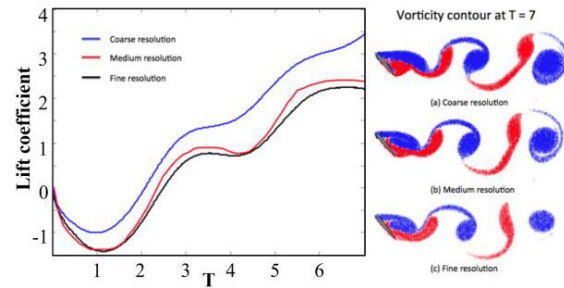


Fig. 1. Left: lift coefficient vs. time history for fixed NACA 0012 at AoA $\alpha = 50^\circ$ and $Re = 1000$.

This convergence study is performed in Fig. 1. The left figure depicts lift coefficient vs. time history for fixed NACA 0012 at AoA $\alpha = 50^\circ$ and $Re = 1000$ while the right figure shows vorticity contours. These contours are colored by blue and red which respectively stand for vortex bubbles shed from leading edge and trailing edge at $T = 7$ (non-dimensional time) for different resolutions of a particle's core size. The results in the figure suggest that the medium size grid provides sufficient resolution to achieve convergence. For the three cases (fine, medium and coarse resolutions), we essentially see sufficiently small differences in the vortical flow in the wake region and the drag coefficients between fine and medium resolutions. Hence, in the rest of the following simulations, the medium resolution is used in order to reduce the memory usage to compute and record the particle's information (vorticity, velocity) while it still maintains the sufficient accuracy.

3. Vortex Identification Methods

Due to the significant roles of vortical structures in turbulence, research for vortex identification has been interesting. It has come up with a number of methods which are designed to identify vortices given the output of simulations or velocity measurements in experiments. Recently, identification of vortices plays an important role for understanding complex flow phenomena. The vortical structures are also found in studies of unsteady laminar separation. In this paper, three vortex identification methods are developed to better understand the separation.

3.1. Vorticity Method

The first vortex identification method is the vorticity field. By using the vortex method the Navier-Stokes equation in terms of vorticity-velocity form is solved, producing a vorticity variable every single time step [11]. The vorticity field will represent the vortical region behind the airfoil. The sign of vorticity indicates a vortex bubble will be shed from the leading edge or trailing edge. Determination of these bubble centers helps evaluate the vortex shedding frequency. Although the centers are difficult to program based on the vorticity ($\omega < 10$), the unsteady laminar separation is well captured. Moreover, the drag force

can be qualitatively estimated based on the size of vorticity scattered in the wake region.

In the first visualization, Fig. 2 shows instantaneous wake contoured by particles vorticity with different AoAs from 30° to 90° at $T = 8$. Blue and red contours stand for vortex bubbles shed from leading edge and trailing edge, respectively. The figure suggests that the laminar separation starts to happen at the $\text{AoA} = 30^\circ$. The unsteady vortices are shed in different frequencies from $\text{AoA} = 30^\circ$ to 90° . The higher AoAs perform the smaller vortex shedding frequencies. Also, the size of the wake and separation bubbles increases from the case of low AoA to high AoA. Hence, the drag force is predicted to be higher in higher AoA. Hence, the vorticity contour only helps to observe the separated unsteady region and predict the drag force.

3.2. Eulerian Method

Due to the stretching nature of unsteady vortical flows, vorticity plays its role in vortex identification less directly than expected. It is usually through the complete information contained in the velocity-gradient tensor. In addition, the vorticity contour mentioned above is not possible to evaluate quantitatively the strengths of the leading edge vortex and trailing edge vortex which helps to compute lift and drag force by using Kelvin's theorem. In order to do that, the following Eulerian methods are essentially suggested to extract more information in terms of near-field separation. Several Eulerian methods for identifying flow structures are considered, see [12], [13]. They are generally formulated in terms of the invariants of the velocity gradient $\nabla \underline{u}$ tensor. These criteria are the iso- surfaces of vorticity, Q -criterion, complex eigenvalues of the velocity gradient tensor, λ_2 and pressure minimum. The work done in [13] showed that the Q -criterion and λ_2 almost give the same flow structures.

In this paper, the Q -criterion is used to identify the core location of vortex wake structure. Moreover, the analysis of the physics of the flow in this section is started by its wake. The Q - criterion is considered following the work listed in [12]. The velocity gradient tensor ∇u is decomposed into the symmetric rate of strain tensor \underline{S} and antisymmetric rate of rotation tensor $\underline{\Omega}$, as

$$\nabla \underline{u} = \underline{S} + \underline{\Omega} \quad (1)$$

where $\underline{S} = \frac{1}{2}(\nabla \underline{u} + \nabla \underline{u}^T)$ and $\underline{\Omega} = \frac{1}{2}(\nabla \underline{u} - \nabla \underline{u}^T)$. The Q - criterion is then defined as

$$Q = \left[\|\underline{\Omega}\|^2 - \|\underline{S}\|^2 \right] > 0 \quad (2)$$

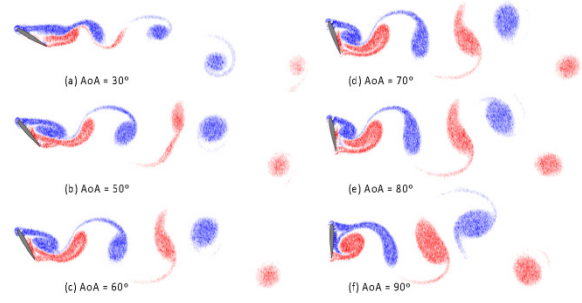


Fig. 2. Instantaneous wake contoured by vorticity values of particles in the flow field with the angles of attack of 30° (a), 50° (b), 60° (c), 70° (d), 80° (e), 90° (f).

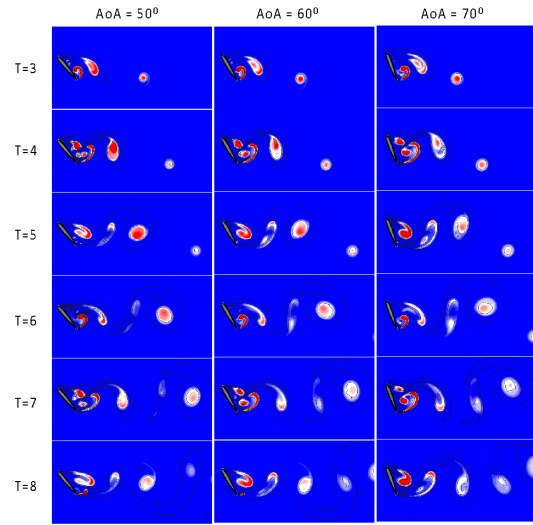


Fig. 3. Snapshots of vorticity contour (black solid lines) versus Q -criterion with three different AoAs (50° , 60° and 70°) at instantaneous times from $T = 3$ to $T = 8$.

A vortex is defined in those regions where $Q > 0$, which is interpreted as a dominance of rotation over strain. In the second visualization,

Fig. 3 shows the snapshots of vorticity contour (black solid lines) vs. Q -criterion (colorful contour) with three different AoAs (50° , 60° and 70°) at instantaneous times from $T = 3$ to $T = 8$. The figure indicates that the unsteady vortical region is remarked by limiting the value of Q -criterion from 0 to 10. Moreover, the leading edge vortex and trailing edge vortex are clearly observed and determined by constraining the value of Q in a range from 8 to 10. Accordingly, the boundary of the leading edge and trailing edge vortex is bounded by the Q value in which the strengths of these vortices are evaluated by taking a sum of absolute strengths of particles in the region where Q values are in the range. The strengths of the leading edge vortex and trailing edge vortex are depicted in Fig. 4.

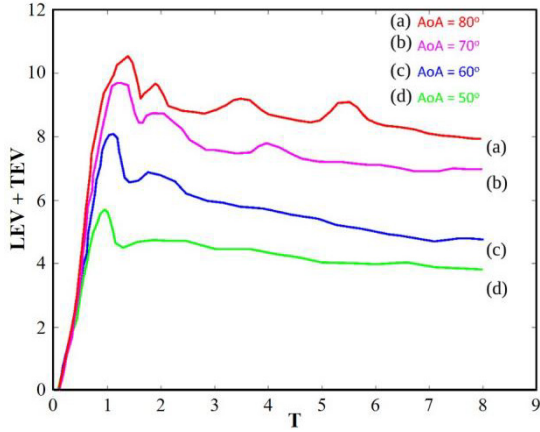


Fig. 4. Time history of summation of vorticity strengths of leading edge vortex and trailing edge vortex developed behind the NACA 0012 at different AoAs (50°, 60°, 70° and 80°).

The time history of summation of vorticity strengths of leading edge vortex and trailing edge vortex developed behind the NACA 0012 at different AoAs. The figure also demonstrates that at the very initial stage of the wake development the strengths are linearly enlarged. Moreover, at the later stage they perform in the same trend in which it reaches a steady state. The figure also demonstrates that the strengths are increased at higher AoAs.

3.3. Lagrangian Method

In the application of flow past high AoA airfoil, flow extends a field of unsteadiness. As complexity arises due to certain flow conditions, such as high AoA, complex geometries or high Reynolds numbers, the need for identifying organizing flow structures is increasingly essential. However, applying the Eulerian methods in these complex flow problems is challenging. For instance, the Q-criterion method only produces the vortical flow region while it is difficult to describe the most stretching, attracting, and shearing material surfaces that form the skeletons of Lagrangian particle dynamics in the far-field wake region. Moreover, it is impossible to identify the separated regions with a vorticity field only.

Lagrangian coherent structures (LCS), which are evaluated by a time-resolved sequence of snapshots of velocity field of an unsteady flow, simply identify regions of large stretching between nearby particles as surfaces in the field of finite time Lyapunov exponents (FTLE) [9]. These surfaces are called “ridges”. FTLE fields are computed using backward time integration of particle grids [14]. The LCS represents attracting material lines and separate regions of separated flow around the airfoil and unsteady flow in the wake.

In order to calculate the FTLE fields in an instantaneous time t , the first step is to initially generate a grid of particles covering the spatial domain of interest. The second step is to advect these particles

backward in time based on the velocity field snapshots computed from the DNS solver. In particular, these snapshots are taken every time step from specified interval time $[t, t - T]$. The option of integration time T , is very significant since it will mark the number of structures during the convection. The third step is to differentiate particle positions after the convection at the time $t - T$ with respect to their initial positions at time t . This finite differencing process will determine the discrete approximation to the Cauchy-Green deformation tensor Δ

$$\Delta = \left(\frac{\partial \phi^T}{\partial \underline{x}} \right)^* \left(\frac{\partial \phi^T}{\partial \underline{x}} \right) \quad (3)$$

where ϕ^T is the flow map (the new positions of particles) after the convection process from t to $t - T$. The notation, the notation * means “transpose”. Based on the map, one Cauchy-Green deformation tensor will represent the deformation of one initial particle. The maximum value of the eigenvalues of Δ identifies one particle trajectory related to the finite time Lyapunov exponent

$$\sigma^T(\underline{x}) = \frac{1}{T} \log \left(\sqrt{\max(\text{eig}(\Delta))} \right) \quad (4)$$

The contour of values of every individual exponent will visualize the whole field of particle trajectories, which will indicate magnitudes of particle stretching ridges in the unsteady region. Although it is simply computed, this method is costly and involves a number of redundant integrations in time for those particles not included in the vortical region. A fast method for FTLE computation has recently been developed to speed up the time-series of FTLE calculations [15]. However, in this paper, since the main purpose is to better understand the unsteady separation, the fast method is not applied yet.

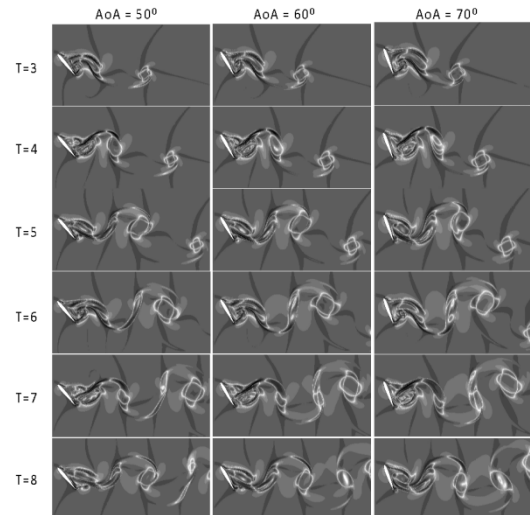


Fig. 5. Snapshots of lagrangian coherent structure with three different AoAs (50°, 60° and 70°) at instantaneous times from $T = 3$ to $T = 8$.

In the following visualizations, FTLE fields measuring stretching in backward time are used to obtain structures that attract particles in forward time. Fig. 5 shows snapshots of Lagrangian coherent structure (contoured by gray color in the range from -0.3 to 10) with three different AoAs (50° , 60° and 70°) at instantaneous times from $T = 3$ to $T = 8$. The LCS was evaluated with particles advected backward in time. The integration time is set to be $T = 0.1$ which is equivalent to 100 time steps. The larger T will take longer time to compute although it shows a higher number of stretching ridges. In Fig. 5, FTLE fields for three interesting cases are depicted, where ridges plotted in white indicate the boundaries of a separation bubble. Specifically, since the flow field is unsteady, for each of the other three unsteady cases, the FTLE ridges are not the same as streamlines. In addition, the periodic vortex shedding cycles are also observed from this figure.

4. Aerodynamic Forces

The aerodynamic forces play an important role to better understand the vortex shedding mechanism shown qualitatively in the previous results. In vortex methods, the classical technique to evaluate the lift and drag force acting on a body is to compute the time derivative of the linear impulse [11]. The linear impulse is based on the vorticity strengths of all particles in the flow field. This method is very robust and has an almost zero computational cost, as it is implemented as a sum running over all particles. Since the DNS solver based on vortex method resolved the flow field with uniform resolution the far wake could become well resolved, thereby the accuracy of linear impulse and forces is retained.

Fig. 6 depicts time history of lift and drag coefficients at different AoAs (50° , 60° , 70° and 80°). The left-hand-side figure shows that at very early stage of the simulation the lift coefficients in the cases of high AoA will be higher than low AoAs from $T = 0$ to $T = 2.25$. From $T = 2.25$ to $T = 8$ the lift coefficients of the cases of lower AoA are monotonically increased. However, the interested region is the later stage of the simulation where the drag and lift coefficient approaches the periodic state. The drag coefficients of the cases of high AoA are higher than low AoA. This also demonstrates the consistency with the observation of the wake size depicted in Fig. 2.

Fig. 7 shows the time history of ratio of lift and drag coefficients at different AoAs (50° , 60° , 70° and 80°). For very early stage of the simulations the figure shows that when the angle of attack is increased, the C_L/C_D ratio rapidly increases from $T = 0$ to $T = 2.25$. Then, as the simulation time goes by from $T = 2.25$ to $T = 8$, the C_L/C_D ratio increases as AoA is lower. Regarding to the later stage of the simulation, the reason for this behavior is that when the angle of attack

is increased until the C_L/C_D ratio reaches its maximum value from $T = 2.25$ to $T = 8$, both C_L and C_D increase but C_L increases more than C_D .

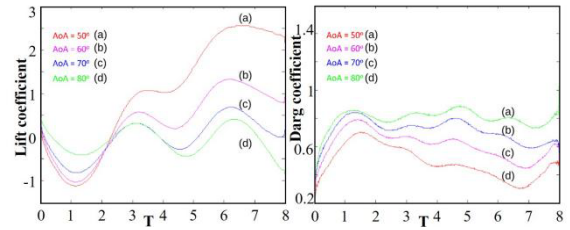


Fig. 6. Time history of lift (left) and drag (right) coefficients at different AoAs (50° , 60° , 70° and 80°).

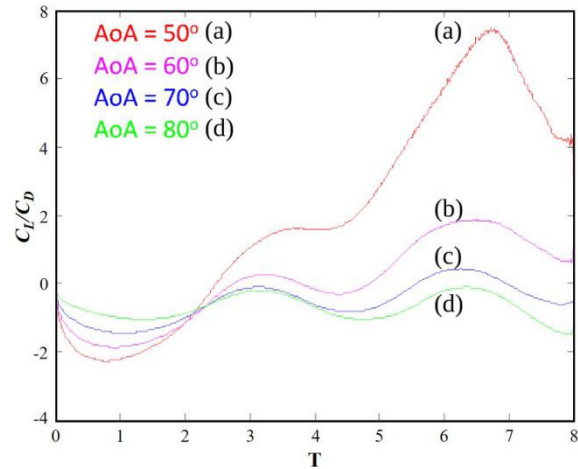


Fig. 7. Time history of ratio of lift and drag coefficients at different AoAs (50° , 60° , 70° and 80°).

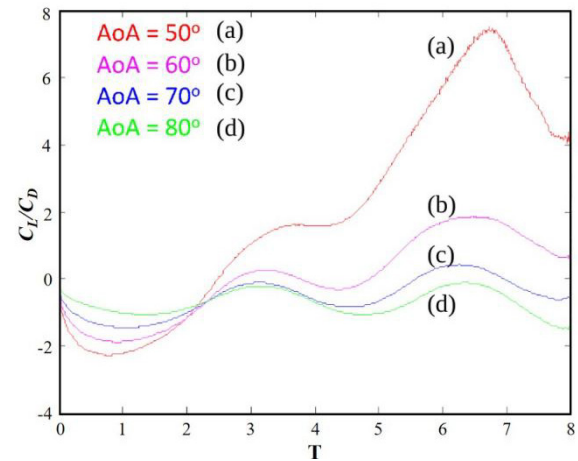


Fig. 8. Lift coefficient versus angles of attack for fixed airfoil NACA 0012 at $Re = 1000$.

Fig. 8 shows average-lift coefficient versus angle of attack for fixed airfoil NACA 0012 at $Re = 1000$. A laminar separation occurs at $\alpha = 30^\circ$. The average post-stall lift, minimum and maximum post-stall lift are presented. For $\alpha > 30^\circ$, a stable limit cycle develops, corresponding to periodic vortex shedding from the leading and trailing edge as shown consistently by Fig. 6 and Fig. 7. At this point, the lift

coefficient still keeps increasing until $\alpha = 47^\circ$ then rapidly decreases from $\alpha \approx 50^\circ$.

5. Conclusion

The unsteady laminar separation on low-Reynolds number airfoil NACA 0012 at high angle of attack using 2D direct numerical simulations based on Lagrangian vortex method have been investigated. The convergence study has been reconfirmed by simulating the unsteady flow over NACA 0012 at angle of attack 50° at three different resolutions ranging from the finest to the coarsest. Three vortex identification methods are also performed in order to extract more information about the unsteady separation process as well as better understand the physics of this process.

1. The first vortex identification method, vorticity contour, is used to capture the vortical region behind the surface in which the package of unsteady vortex bubbles is observed in different angles of attack. However, for determination of the centers of these bubbles, this method is difficult to track in the flow field.

2. The second vortex identification method, Q -criterion, has shown the advantages in order to capture the vortical region and track the near-wall separation by recording the vortex strengths of leading edge vortex and trailing edge vortex at high angle of attacks. The time history of the strengths has shown a good agreement to the time history of drag coefficient.

3. The third vortex identification method, Lagrangian coherent structure, has shown its strength to record the most stretching, attracting, and shearing material surfaces that form the skeletons of Lagrangian particle dynamics in the far-field wake region. Accordingly, the tracking of particles in high shear surfaces is well captured. It is observed that the FTLE ridges are unsteady and periodic as a vorticity field. In addition, Velocity field snapshots from DNS are used to extract FTLE to visualize relevant flow structures.

References

- [1] Ifjuand, P. G., Jenkins, A. D., Ettingers, S., Lian, Y., & Shyy, W., Flexible-wing- based micro air vehicles, AIAA, pp. 2002-0705, 2002.
<https://doi.org/10.2514/6.2002-705>
- [2] Jones, K. D., & Platzer, F. M., Bio-inspired design of flapping-wing micro air vehicles-an engineers perspective, AIAA, pp. 2006-0037, 2006.
<https://doi.org/10.2514/6.2006-37>
- [3] Ellington, C., The novel aerodynamics of insect flight: Applications to micro-air vehicles, Journal of Experimental Biology, Vol. 202, pp. 3439-3448, 1999.
<https://doi.org/10.1242/jeb.202.23.3439>
- [4] Diwan, S. S., & Ramesh, O. N., Laminar separation bubbles: Dynamics and control, Sadhana, Vol. 32, pp. 103-109, 2007.
<https://doi.org/10.1007/s12046-007-0009-7>
- [5] Dickinson, M. H., & Gotz, K. G., Unsteady aerodynamic performance of model wings at low Reynolds numbers, Journal of Experimental Biology, Vol. 174, pp. 45-64, 1993.
<https://doi.org/10.1242/jeb.174.1.45>
- [6] Dung, D. V., Lavi, R. Z., & Muhammad, H., Two-dimensional fast Lagrangian vortex method for simulating flows around a moving boundary, Journal of Mechanical Engineering, Vol. 12, No. 1, pp. 31-46, 2015.
- [7] Green, M. A., Rowley, C. W., & Haller, G., Detection of Lagrangian coherent structures in three-dimensional turbulence, Journal of Fluid Mechanics, Vol. 572, pp. 111-120, 2007.
<https://doi.org/10.1017/S0022112006003648>
- [8] Jakobsson, J., Investigation of Lagrangian coherent structures-To understand and identify turbulence, Dissertation, Chalmers University of Technology, Sweden, 2012.
- [9] Haller, G., Lagrangian coherent structures from approximate velocity data, Physics of Fluids, Vol. 14, No. 6, pp. 1851-1861, 2002.
<https://doi.org/10.1063/1.1477449>
- [10] Lipinski, D., Cardwell, B., & Mohseni, K., A Lagrangian analysis of a two-dimensional airfoil with vortex shedding, Journal of Physics A: Mathematical and Theoretical, Vol. 41, No. 34, 2008.
<https://doi.org/10.1088/1751-8113/41/34/344011>
- [11] Ploumhans, P., & Winckelmans, G. S., Vortex methods for high-resolution simulations of viscous flow past bluff bodies of general geometry, Journal of Computational Physics, Vol. 165, No. 2, pp. 354-406, 2000.
<https://doi.org/10.1006/jcph.2000.6614>
- [12] Hunt, J. C. R., Wray, A., & Moin, P., Eddies, stream, and convergence zones in turbulent flows, Center for turbulence research report CTR-S88, pp. 193-208, 1988.
- [13] Chakraborty, P., Balachandar, S., & Adrian, R. J., On the relationships between local vortex identification schemes, Journal of Fluid Mechanics, Vol. 535, pp. 189-214, 2005.
<https://doi.org/10.1017/S0022112005004726>
- [14] Germer, T., Lagrangian coherent structures with guaranteed material separation, Computer Graphics Forum, Vol. 30, No. 3, 2011.
<https://doi.org/10.1111/j.1467-8659.2011.01925.x>
- [15] Brunton, S. L., & Rowley, C. W., Fast computation of FTLE fields for unsteady flows: a comparison of methods, Chaos, Vol. 20, No. 1, 2010.
<https://doi.org/10.1063/1.3270044>